Electronic Supporting Information

Cobalt-Manganese Modified Theophrastite Phase of Nickel Hydroxide Nanoflower Arrays on Nickel Foam as self-standing Bi-functional Electrode for Overall Water Electrolysis.

Geeta Pandurang Kharabe,[a, b†] Rajith Illathvalappil,[a, b†] Sidharth Barik,[a, b] Fayis Kanheerampockil,[c, b] Priyanka S. Walko,[d, b] Suresh K. Bhat,[c, b] R. Nandini Devi,[d, b] and Sreekumar Kurungot,*[a, b]

(a) Geeta Pandurang Kharabe, Dr. Rajith Illathvalappil, Sidharth Barik, Dr. Sreekumar Kurungot
Physical & Materials Chemistry Division, CSIR-National Chemical Laboratory. Pune, Maharashtra, 411008 (India); Email: k.sreekumar@ncl.res.in

(b) Geeta Pandurang Kharabe, Dr. Rajith Illathvalappil, Sidharth Barik Priyanka S. Walko, Fayis Kanheerampockil, Dr. Suresh K. Bhat, Dr. R. Nandini Devi, Dr. Sreekumar Kurungot
Academy of Scientific and Innovative Research, Postal Staff College Area, Kamla Nehru Nagar, Ghaziabad, Uttar Pradesh-201002, India.

[c] Fayis Kanheerampockil, Dr. Suresh K. Bhat
Polymer Science and Engineering Division
CSIR–National Chemical Laboratory, Pune, Maharashtra, 411008 (India)

(d) Priyanka S. Walko, Dr. R. Nandini Devi
Catalysis and Inorganic Chemistry Division
CSIR–National Chemical Laboratory, Pune, Maharashtra, 411008 (India)

† These authors contributed equally to this work.

Table and Contents

1. Experimental:

1.1. Details of GC specifications

The amount of H_2 and O_2 evolved was determined using gas chromatography (5700 Nucon gas chromatograph with Carbosphere column and Ar as carrier gas) with a thermal conductivity detector. The program used in GC for all the analyses involved the detector temperature of 100 ºC and oven temperature of 50 ºC at the time of injection. A gas phase syringe (injection volume of 500 µL).

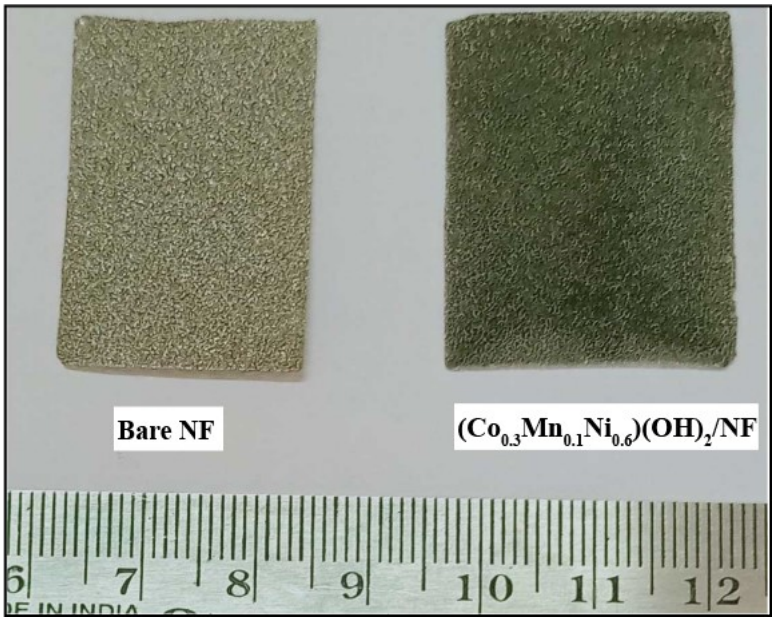

Figure S1. Digital photograph of Bare NF and $(Co_{0.3}Mn_{0.1}Ni_{0.6})(OH)_2$/NF.

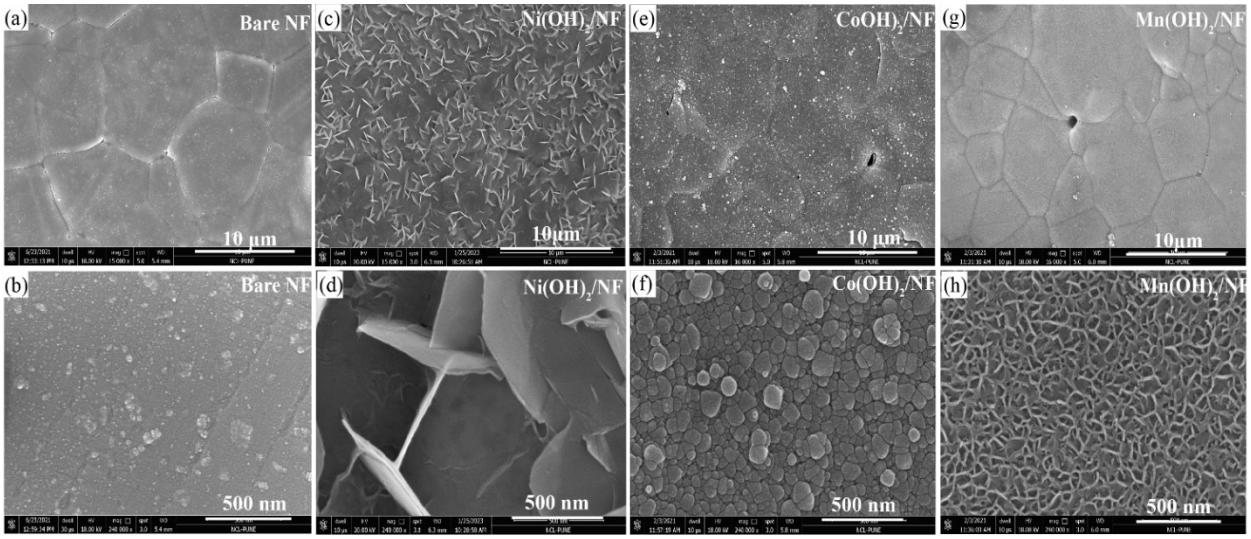

Figure S2. The FE-SEM images recorded at different magnifications of (a-b) Bare NF, (c-d) $Ni(OH)_2$/NF, (e-f) $Co(OH)_2$/NF, and (g-h) $Mn(OH)_2$/NF.

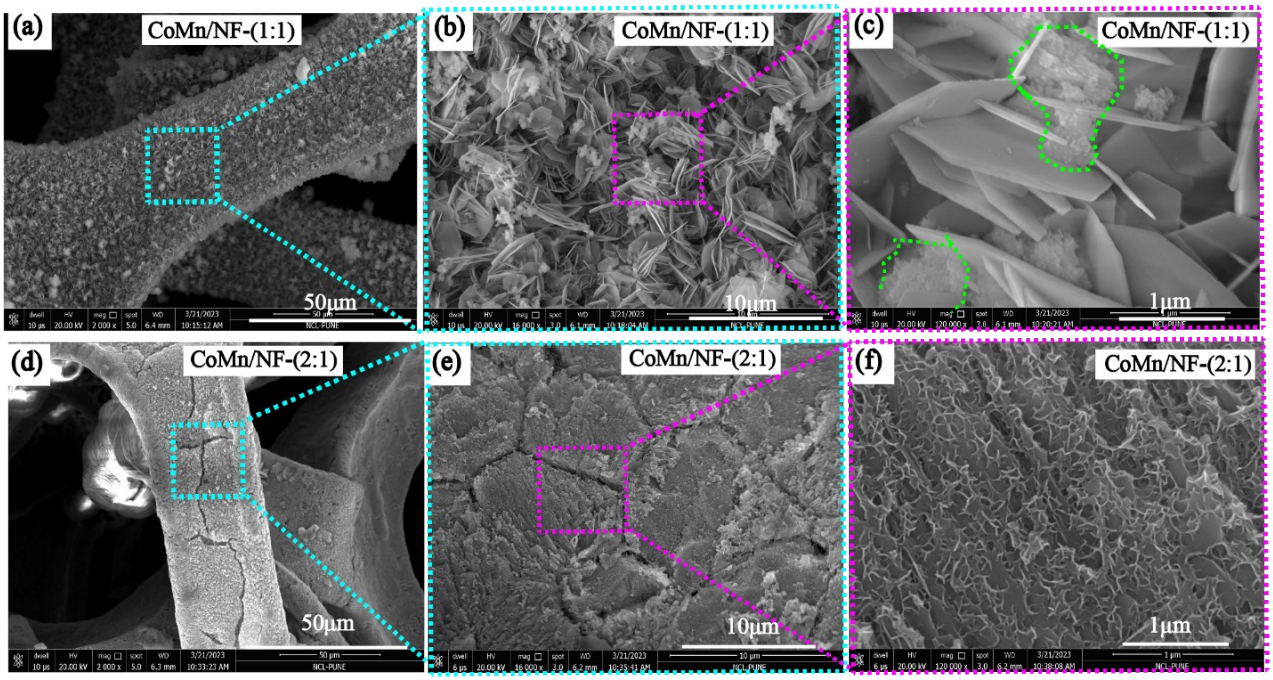

Figure S3. . FE-SEM images: (a) the relatively rough surface of (CoMn)/NF-(1:1), (b) the magnified image of the portion marked in the square in (a), (c) the sheet-like morphology with randomly oriented structure, (d) the rough surface morphology of (CoMn)/NF-(2:1), (e) the magnified image of the portion marked in the square in (d) and (f) the high-magnified image of (CoMn)/NF-(2:1) with the stacked-type morphology.

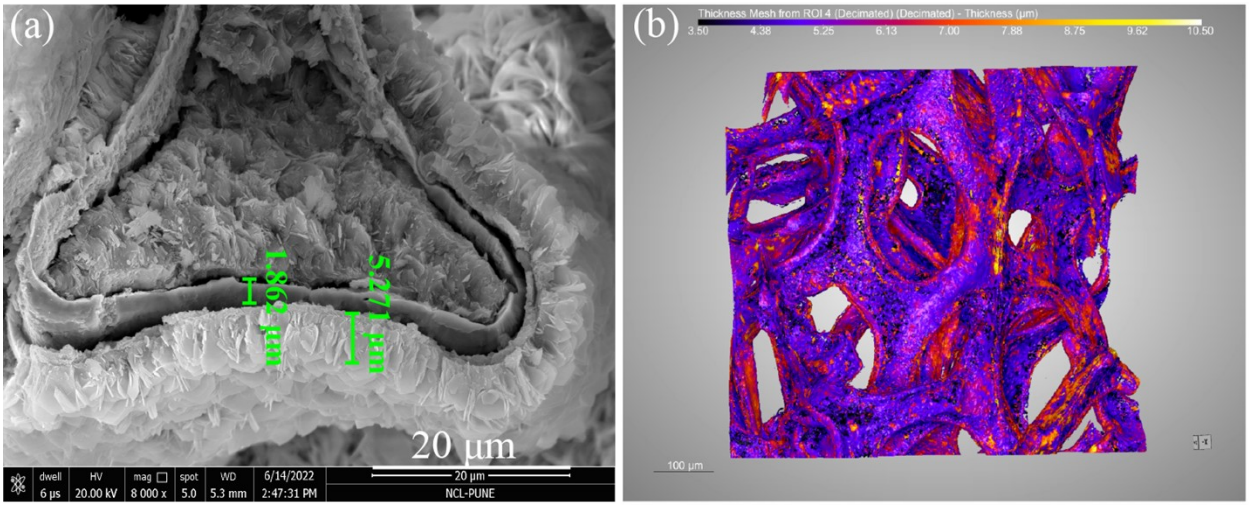

Figure S4. (a) FESEM and (b) colour-coded thickness profile obtained from the tomography images of $(Co_{0.3}Mn_{0.1}Ni_{0.6})(OH)_2$/NF.

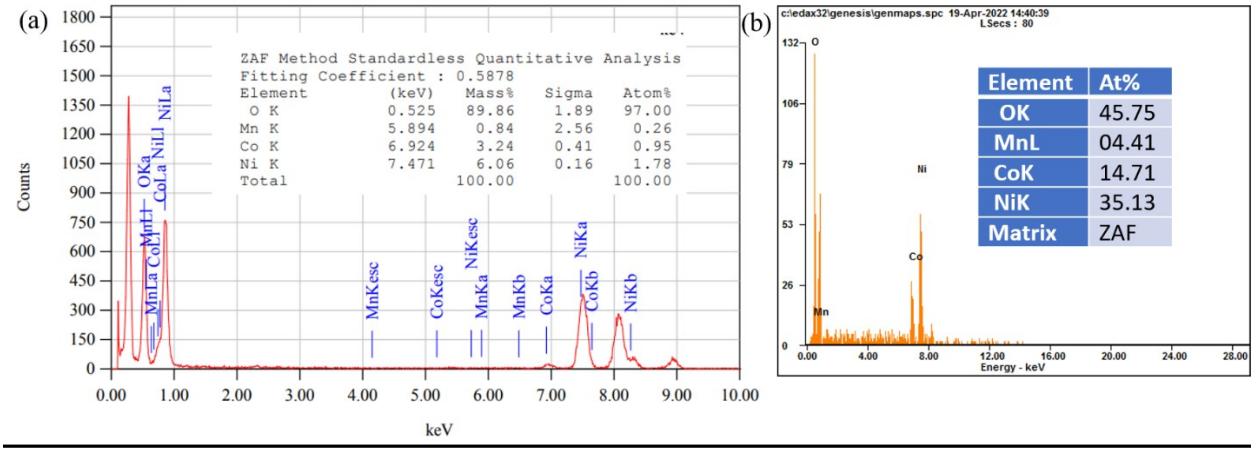

Figure S5: (a) HR-TEM-EDX of $(Co_{0.3}Mn_{0.1}Ni_{0.6})(OH)_2$/NF and (b) SEM-EDX of $(Co_{0.3}Mn_{0.1}Ni_{0.6})(OH)_2$/NF.

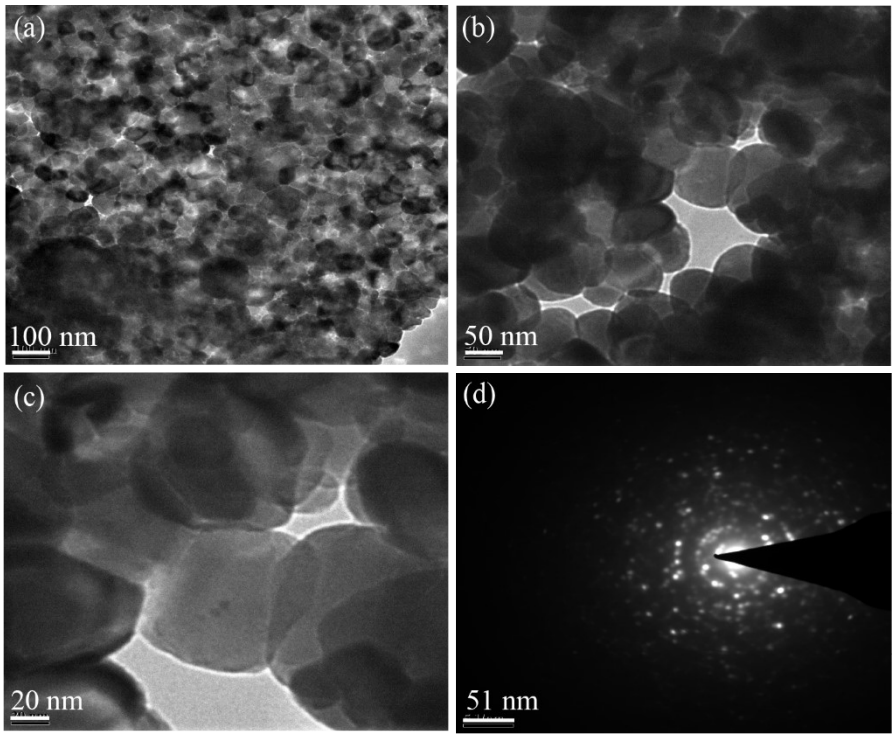

Figure S6. (a-c) TEM images of $Co(OH)_2$/NF recorded at different magnifications and (d) the corresponding SAED pattern.

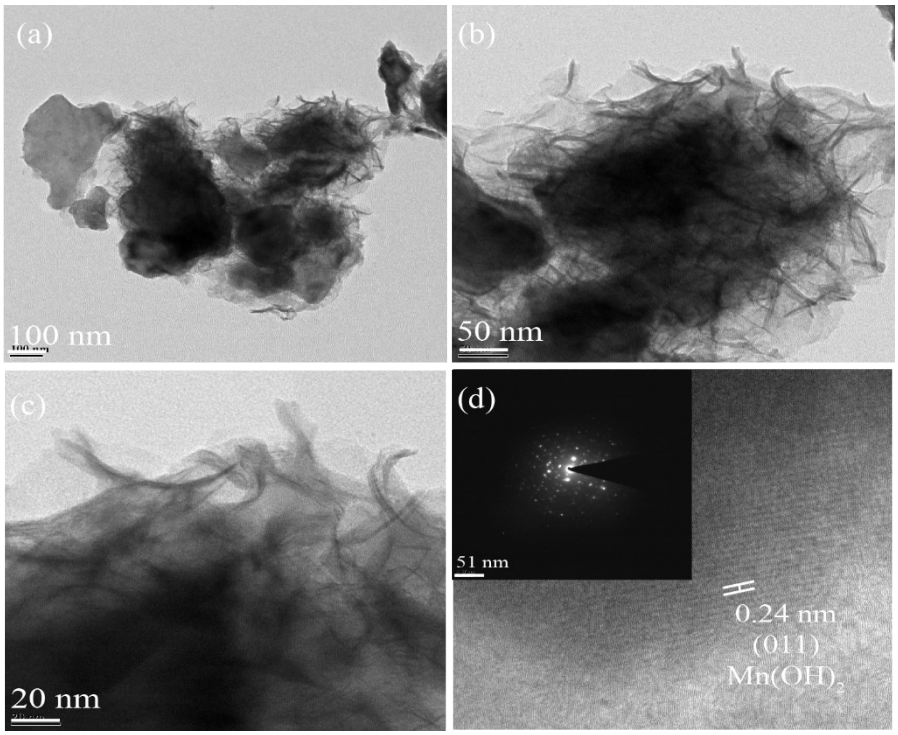

Figure S7. (a-c) TEM images of $Mn(OH)_2$/NF recorded at different magnifications and (d) inset shows SAED pattern of $Mn(OH)_2$/NF indicates the crystalline nature.

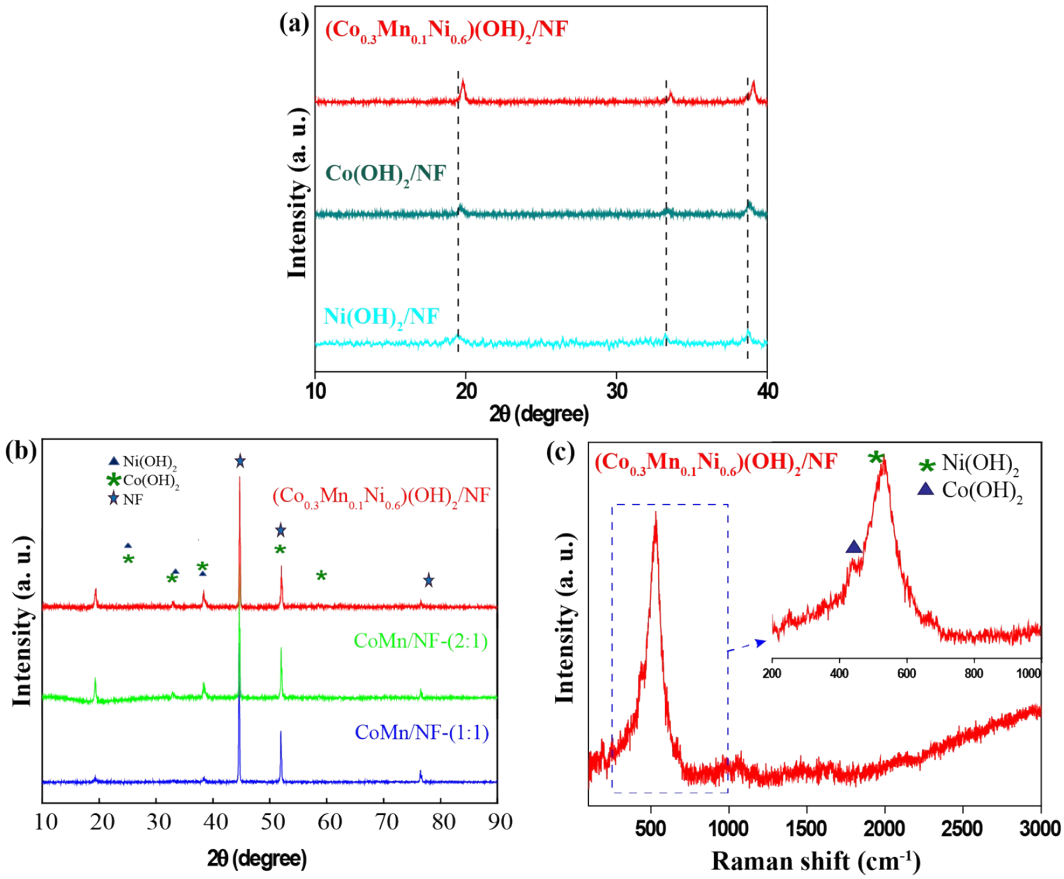

Figure S8. (a) Comparative XRD patterns of $(Co_{0.3}Mn_{0.1}Ni_{0.6})(OH)_2$/NF, $Co(OH)_2$/NF, and $Ni(OH)_2$/NF, (b) comparative XRD profiles of $(Co_{0.3}Mn_{0.1}Ni_{0.6})(OH)_2$/NF, CoMn/NF-(1:1) and CoMn/NF-(2:1), and (c) Raman spectrum of $(Co_{0.3}Mn_{0.1}Ni_{0.6})(OH)_2$/NF.

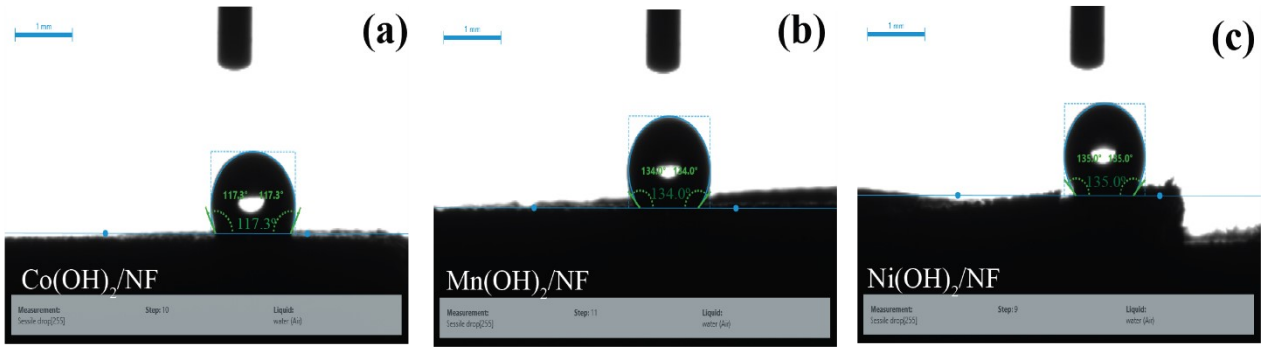

Figure S9: The contact angle measurement of (a) $Co(OH)_2$/NF, (b) $Mn(OH)_2$/NF, and (c) $Ni(OH)_2$/NF.

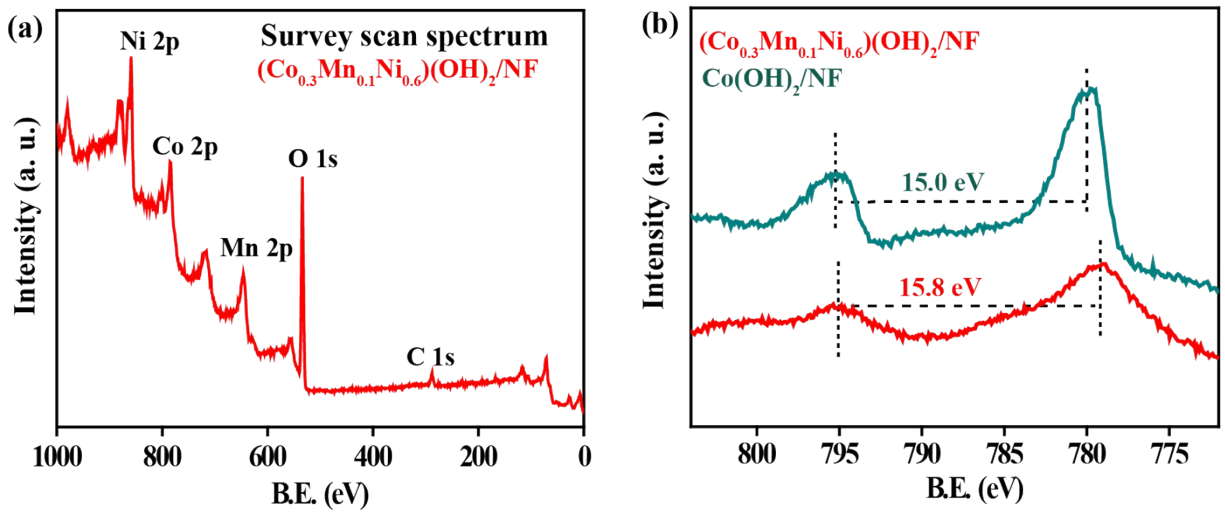

Figure S10: (a) XPS survey spectrum of $(Co_{0.3}Mn_{0.1}Ni_{0.6})(OH)_2$/NF, and (b) the comparative XPS spectra of Co 2p in $Co(OH)_2$/NF and $(Co_{0.3}Mn_{0.1}Ni_{0.6})(OH)_2$/NF with the spin splitting values.

OER Reaction Pathway:

$$4OH \rightarrow O_{2(g)} + 2H_2O(l) + 4e^-$$

The OER reaction mechanism in the alkaline medium follows three elementary steps:

$$M + OH^- \rightarrow M - O + e^-$$

$$M - OH + OH^- \rightarrow M - O + 2H_2O(l) \; e^-$$

$$M - O + OH^- \rightarrow MOOH + e^-$$

$$MOOH + OH^- \rightarrow M + O_{2(g)} + H_2O(l) \; e^-$$

The HER Reaction Pathway:

The general HER mechanism in the alkaline medium follows three elementary steps:

Volmer step:

$$2H_2O + M + 2e^- \rightleftarrows 2M - OH + H_{ad} + 2OH^-$$

Second Heyrovsky step:

$$H_20 + M - H_{ad} + e^- \rightleftarrows M + H_2 + OH^-$$

Or the Tafel recombination step:

$$2M - H_{ad} \rightleftarrows 2M + H_2$$

1.2. The Hg/HgO reference electrode calibration and conversion to RHE:

The Hg/HgO electrode was calibrated according to our previous report.[1] By utilizing a 3-electrode setup consisting of a platinum RDE electrode, graphite rod, and Hg/HgO as the working electrode (WE), counter electrode (CE), and reference electrode (RE), respectively, in an H_2-saturated 1M KOH electrolyte. The potential when the current crossed the zero point during the linear sweep voltammogram (LSV) measurement at a scan rate of 0.50 mV/s was taken as the thermodynamic potential for the hydrogen electrode reactions. This potential in the present case was found to be at 0.913 V. Henceforth, for the conversion of the voltage recorded as for Hg/HgO to the RHE scale, the below equation is used:

E (RHE) = E (Hg/HgO) + 0.913 V …….1

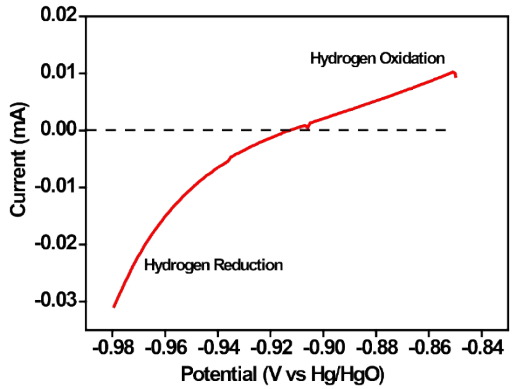

Figure S11. Calibration of Hg/HgO reference electrode in 1 M KOH solution.

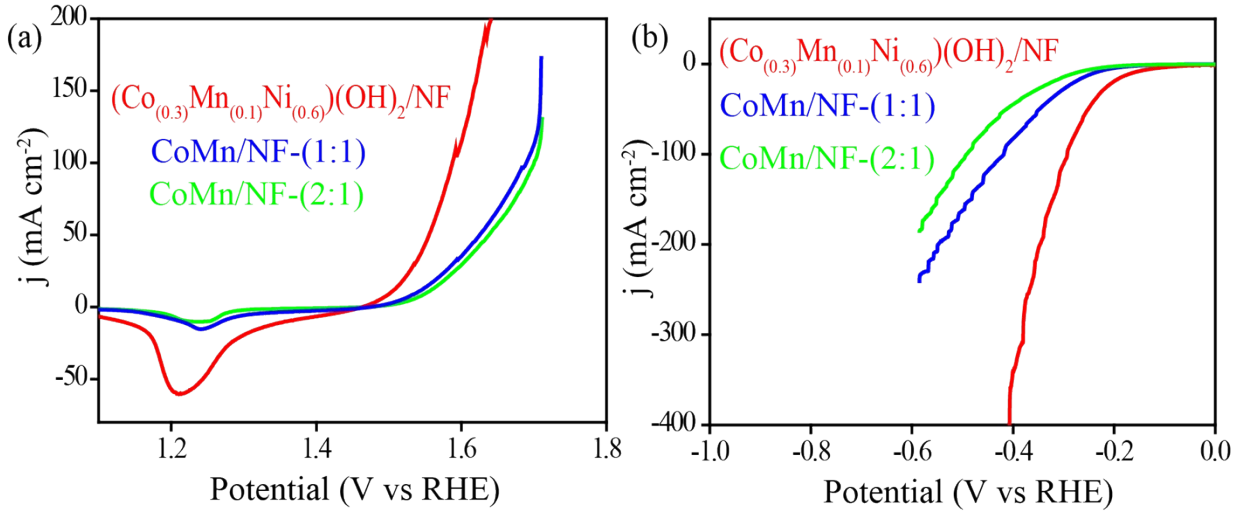

Figure S12. (a) The OER polarisation plots of $(Co_{0.3}Mn_{0.1}Ni_{0.6})(OH)_2$/NF, CoMn/NF-(1:1) and CoMn/NF-(2:1) performed in 1 M KOH electrolyte, (b) the HER polarisation plots of $(Co_{0.3}Mn_{0.1}Ni_{0.6})(OH)_2$/NF, CoMn/NF-(1:1) and CoMn/NF-(2:1) performed in 1 M KOH electrolyte.

Table S1: Comparison of the OER, HER and the overall water-splitting activities of the $(Co_{0.3}Mn_{0.1}Ni_{0.6})(OH)_2$ /NF, CoMn/NF-(1:1) and CoMn/NF-(2:1).

Sr. No.	**Electrocatalyst**	**Electrolyte**	**OER Potential (mV) @ 10mA cm^{-2}**	**HER Potential (mV) @ 10 mA cm^{-2}**	**OWS Potential (V) @ 10mA cm^{-2}**
1.	CoMn/NF-(1:1)	1 M KOH	310	242	1.75
2.	CoMn/NF-(2:1)	1 M KOH	320	286	1.81
3.	$(Co_{0.3}Mn_{0.1}Ni_{0.6})(OH)_2$/NF	1 M KOH	270	163	1.62

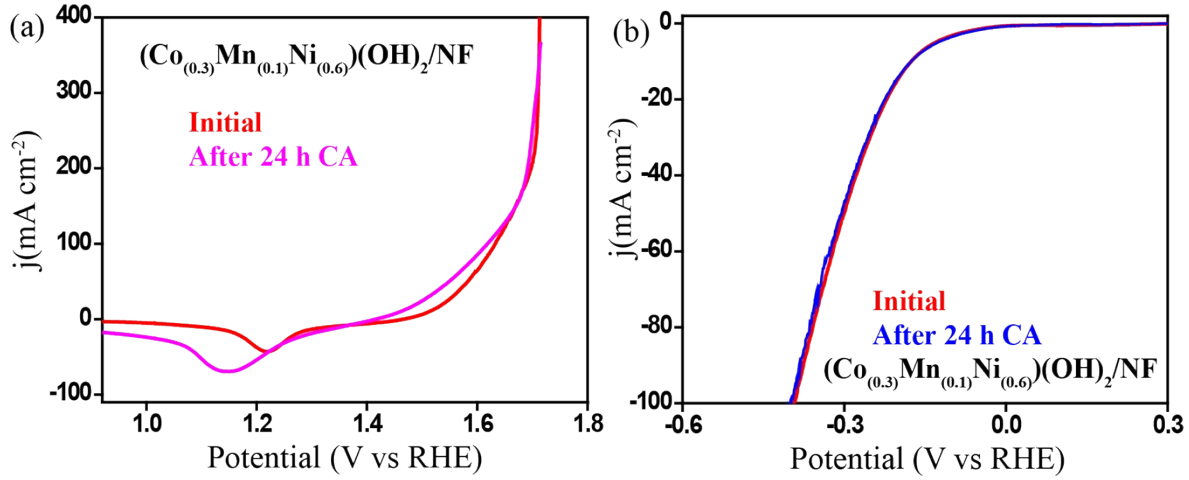

Figure S13: The comparative LSVs of $(Co_{0.3}Mn_{0.1}Ni_{0.6})(OH)_2$/NF recorded in 1M KOH before and after the stability testing: (a) OER and (b) HER.

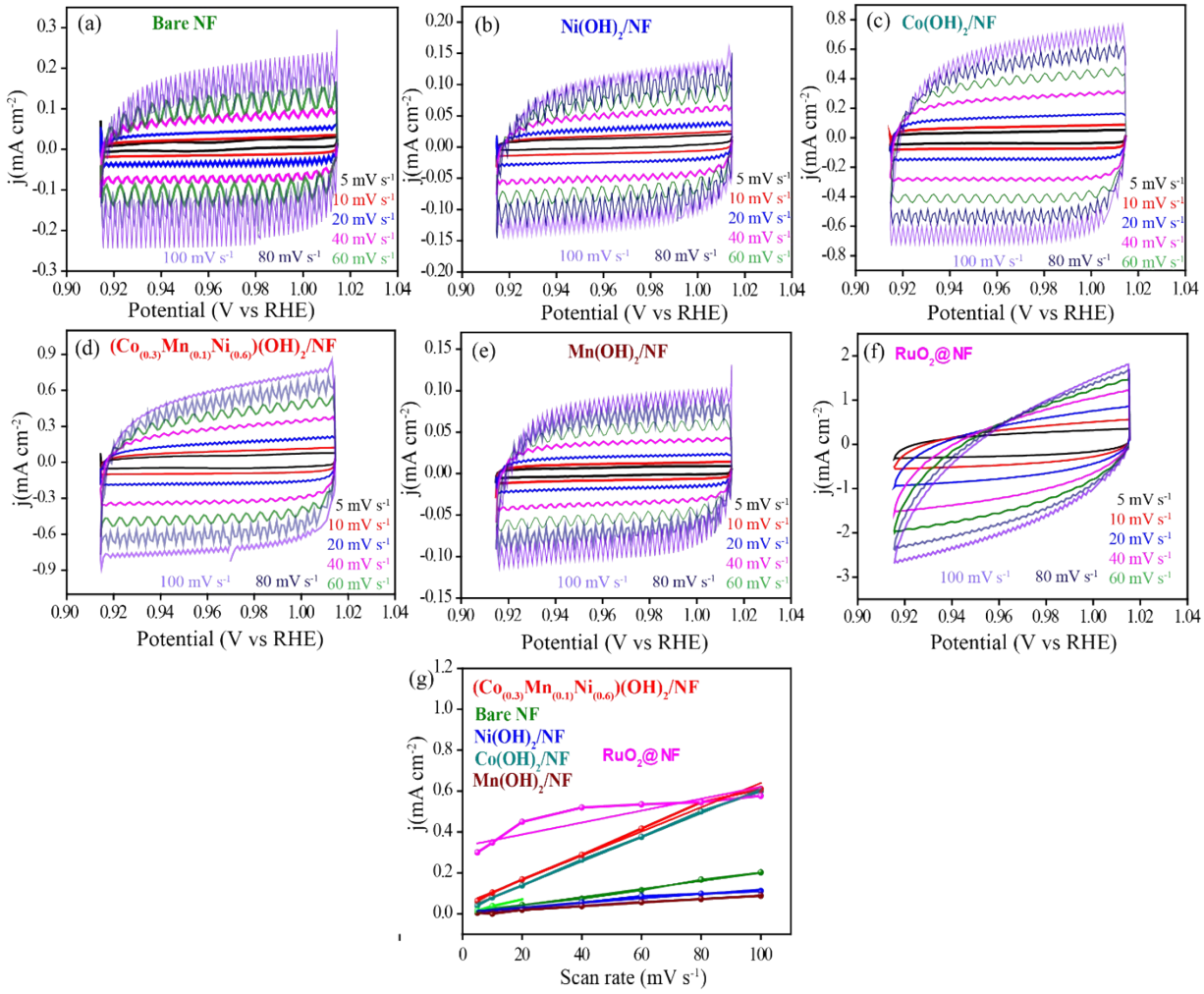

Figure S14. The cyclic voltammograms recorded at different scan rates: (a) Bare NF, (b) $Ni(OH)_2$/NF, (c) $Co(OH)_2$/NF, (d) $(Co_{0.3}Mn_{0.1}Ni_{0.6})(OH)_2$/NF, (e) $Mn(OH)_2$/NF, (f) RuO_2@NF, and (g) the plots of the cathodic current density against the scan rate in the non-Faradaic region of 0.915 to 1.015 V *vs*. RHE.

Table S2. The C_{dl} values recorded for OER.

Sample	Cdl $_{OER}$ (mF cm^{-1})
Bare NF	1.9
$Ni(OH)_2$/NF	1.1
$Co(OH)_2$/NF	5.8
$Mn(OH)_2$/NF	0.91

$Co_{(0.3)}Mn_{(0.1)}Ni_{(0.6)}(OH)_2$/NF	5.92
RuO_2@NF	2.91

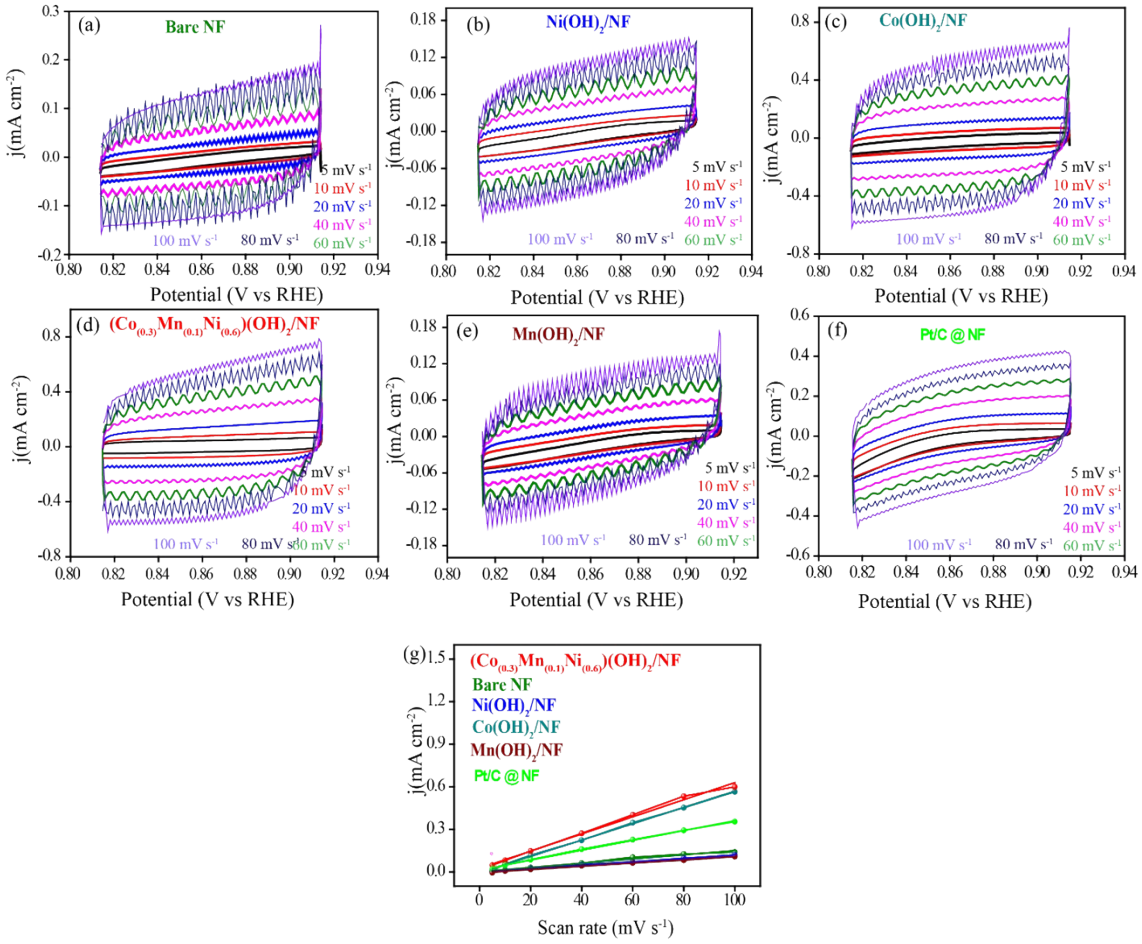

Figure S15. The cyclic voltammograms recorded at different scan rates: (a) Bare NF, (b) $Ni(OH)_2$/NF, (c) $Co(OH)_2$/NF, (d) $(Co_{0.3}Mn_{0.1}Ni_{0.6})(OH)_2$/NF, (e) $Mn(OH)_2$/NF, (f) Pt/C@NF, and (g) the plots of the cathodic current density against the scan rate in the non-Faradaic region of 0.915 to 0.815 V *vs*. RHE.

Table S3. The C_{dl} values recorded for HER

Sample	Cdl $_{HER}$ (mF cm^{-1})
Bare NF	1.49

$Ni(OH)_2$/NF	1.23
$Co(OH)_2$/NF	5.75
$Mn(OH)_2$/NF	1.14
$Co_{(0.3)}Mn_{(0.1)}Ni_{(0.6)}(OH)_2$/NF	6.03
Pt/C@NF	3.48

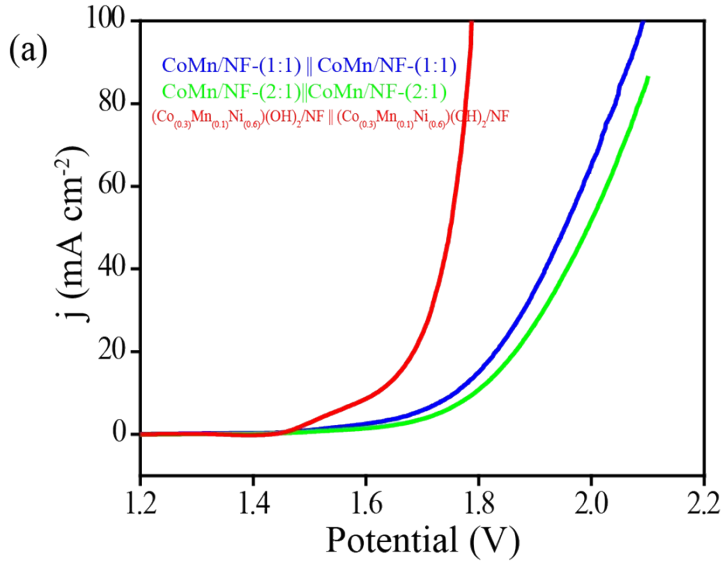

Figure S16. The comparative LSV plots corresponding to the overall water splitting of $(Co_{0.3}Mn_{0.1}Ni_{0.6})(OH)_2$/NF, CoMn/NF-(1:1) and CoMn/NF-(2:1).

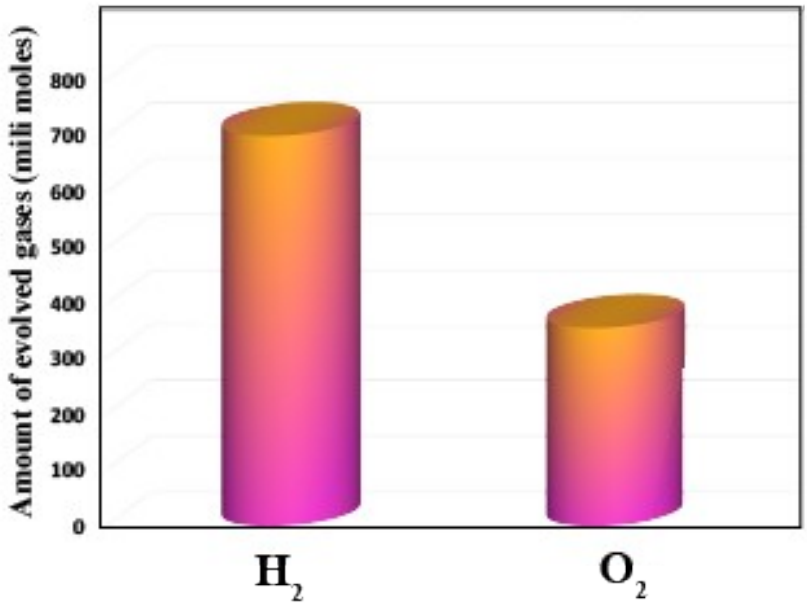

Figure S17. Gas chromatography analysis: the bar diagram shows the amount of the evolved hydrogen and oxygen during the water electrolysis using $(Co_{0.3}Mn_{0.1}Ni_{0.6})(OH)_2$/NF as the anode and cathode.

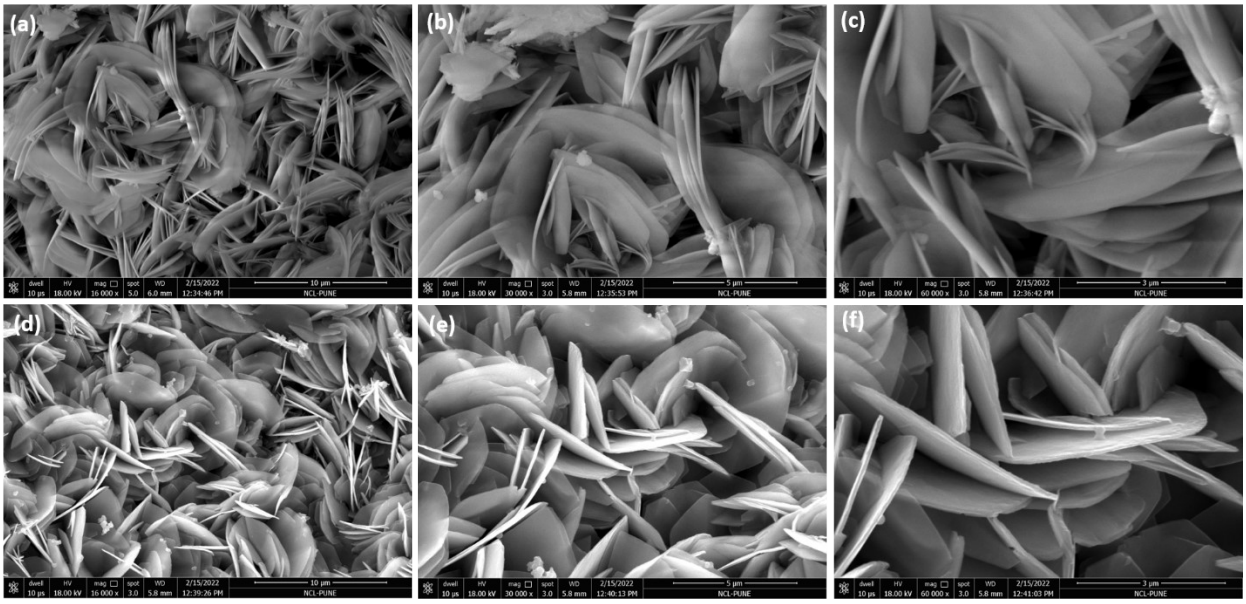

Figure S18. Post-analysis of the electrodes after the overall water-splitting experiment: (a, b, c) the $(Co_{0.3}Mn_{0.1}Ni_{0.6})(OH)_2$/NF anode and (d, e, f) the $(Co_{0.3}Mn_{0.1}Ni_{0.6})(OH)_2$/NF cathode.

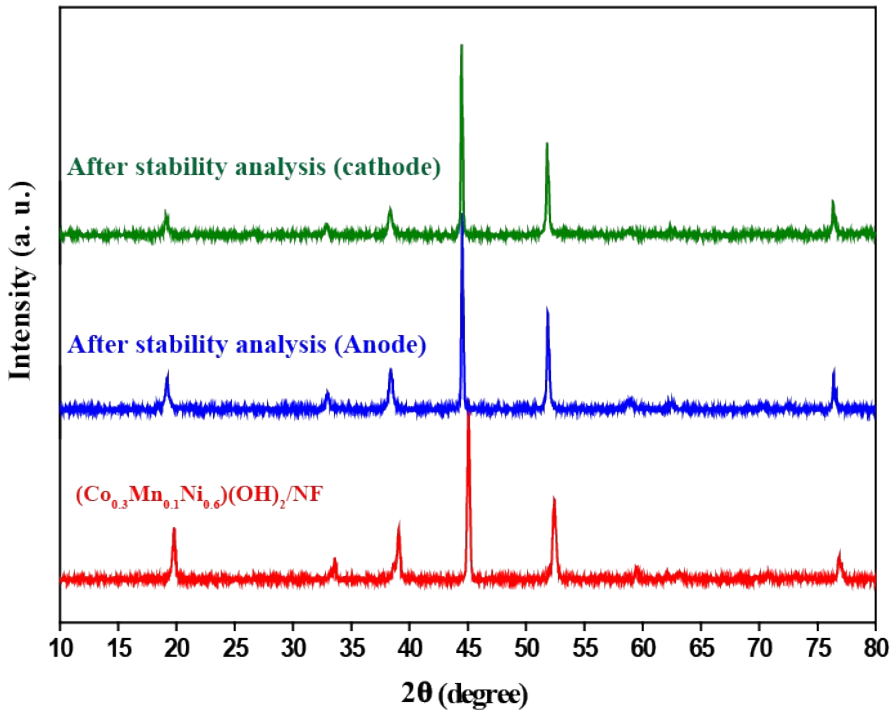

Figure S19. Post-analysis of the electrodes after the overall water-splitting experiment of the $(Co_{0.3}Mn_{0.1}Ni_{0.6})(OH)_2$/NF anode (red) and cathode (green).

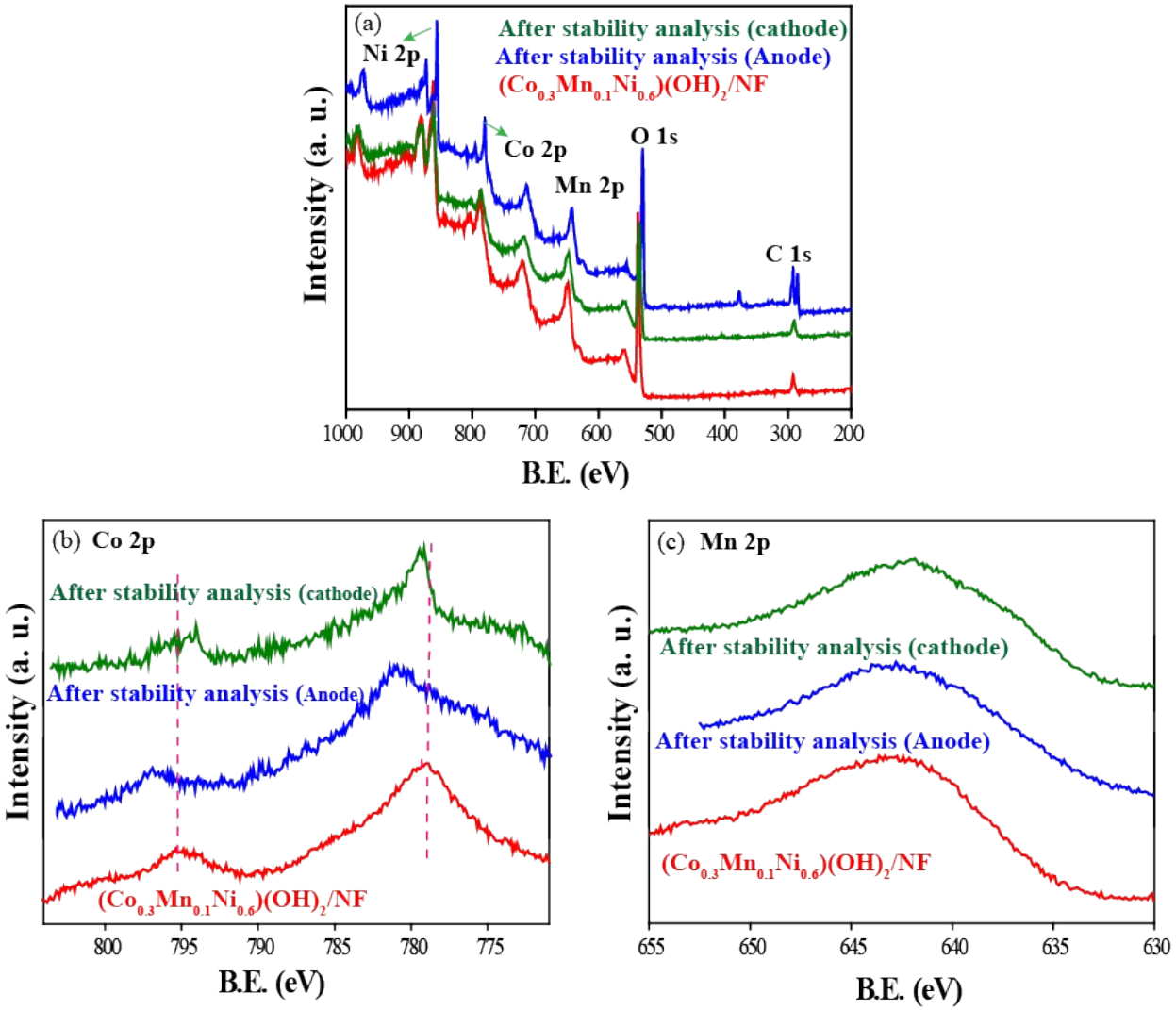

Figure S20. Post-analysis of the electrodes after the overall water-splitting: (a) survey scan spectra, (b) the Co 2p of the $(Co_{0.3}Mn_{0.1}Ni_{0.6})(OH)_2$/NF (red), anode after stability (blue) and cathode after stability (green) and (c) the Mn 2p $(Co_{0.3}Mn_{0.1}Ni_{0.6})(OH)_2$/NF (red) anode after stability (blue) and cathode after stability (green).

Table S4: Comparison of the OER, HER and overall water-splitting activities of the reported systems *vs* the in-house system.

Sr. No.	Electrocatalyst	Electrolyte	OER Potential @ 10mA cm^{-2}	HER Potential @ 10mA cm^{-2}	Potential @ 10mA cm^{-2}	References
1.	NiCo–$NiCoO_2$@NC	1 M KOH	318 mV	94 mV	1.44 V	[2]
2.	CoS/$Co(OH)_2$@MoS_2	1 M KOH	380 mV	143 mV	1.58 V	[3]
3.	VCoCOx@NF	1 M KOH	240 mV	63 mV	1.54 V	[4]
4.	Ni/Ni(OH)2-$NiCo_2O_4$/NF	1 M KOH	235 mV	53 mV	1.51 V	[5]
5.	$Ni(OH)_2$@Ni/CC	1 M KOH	-	-	1.58 V	[6]
6.	Al-CoP/CC	1 M KOH	265 mV	52 mV	1.56 V	[7]
7.	Ni/Ni_8P_3	1 M KOH	270 mV @ 30 mA cm^{-2}	130 mV	1.61 V	[8]
8.	Co_3O_4-MTA/NF	1 M NaOH	152 mV	98 mV	1.63 V	[9]
9.	$NixCo_3$−xO4 ‖ NiCo/NiCoOx	1 M KOH	337 mV	155 mV	1.75 V	[10]
10.	NiCoP/NF	1 M KOH	308 mV@ 50 mA cm^{-2}	133 mV@ 50 mA cm^{-2}	1.77 V	[11]
11.	**$(Co_{0.3}Mn_{0.1}Ni_{0.6})(OH)_2$/ NF**	**1 M KOH**	**270 mV**	**163 mV**	**1.62 V**	**This work**

`

2. References

1. S. K. Singh, V. Kashyap, N. Manna, S. N. Bhange, R. Soni, R. Boukherroub, S. Szunerits and S. Kurungot, *ACS Catal.*, 2017, **7**, 6700-6710.
2. Y. Xiao, P. Zhang, X. Zhang, X. Dai, Y. Ma, Y. Wang, Y. Jiang, M. Liu and Y. Wang, *J. Mater. Chem. A*, 2017, **5**, 15901-15912.
3. T. Yoon and K. S. Kim, *Adv. Funct. Mater.*, 2016, **26**, 7386-7393.
4. A. Meena, P. Thangavel, A. S. Nissimagoudar, A. Narayan Singh, A. Jana, D. Sol Jeong, H. Im and K. S. Kim, *Chem. Eng. J.*, 2022, **430**, 132623.
5. Y. Yu, C. Chen, Y. Liu, H. Yu, S. Li, Y. Xue, N. Cai, J. Wang and F. Yu, *J. Mater. Chem. C*, 2022, **126**, 5493–5501.
6. Z. Xing, L. Gan, J. Wang and X. Yang, *J. Mater. Chem. A*, 2017, **5**, 7744-7748.
7. R. Zhang, C. Tang, R. Kong, G. Du, A. M. Asiri, L. Chen and X. Sun, *Nanoscale*, 2017, **9**, 4793-4800.
8. G.-F. Chen, T. Y. Ma, Z.-Q. Liu, N. Li, Y.-Z. Su, K. Davey and S.-Z. Qiao, *Adv. Funct. Mater.*, 2016, **26**, 3314-3323.
9. Y. P. Zhu, T. Y. Ma, M. Jaroniec and S. Z. Qiao, *Angew.Chem.Int.Ed.*, 2017, **56**, 1324-1328.
10. X. Yan, K. Li, L. Lyu, F. Song, J. He, D. Niu, L. Liu, X. Hu and X. Chen, *ACS Appl. Energy Mater*, 2016, **8**, 3208-3214.
11. Y. Li, H. Zhang, M. Jiang, Y. Kuang, X. Sun and X. Duan, *Nano Res.*, 2016, **9**, 2251-2259.